Journal of the Korean Nuclear Society
Volume 33, Number 6, pp.566~584, December, 2001

Evaluation of Creep-Fatigue Damage of KALIMER Reactor Internals Using the Elastic Analysis Method in RCC-MR

Gyeong-Hoi Koo and Bong Yoo

Korea Atomic Energy Research Institute
150 Dukjin-dong, Yusong-gu, Taejon 305-353, Korea
ghkoo@kaeri.re.kr

(Received Februry 8, 2001)

Abstract

In this paper, the progressive deformation and the creep-fatigue damage for the conceptually designed reactor internals of KALIMER(Korea Advanced LIquid MEtal Reactor) are carried out by using the elastic analysis method in the RCC-MR code for normal operating conditions including the thermal load, seismic load (OBE) and dead weight. The maximum operating temperature of this reactor is 530℃ and the total service lifetime is 30 years. Thus, the time-dependent creep and stress-rupture effects become quite important in the structural design. The effects of the thermal induced membrane stress on the creep-fatigue damage are investigated with the risk of the elastic follow-up. To calculate the thermal stress, detailed thermal analyses considering conduction, convection and radiation heat transfer mechanisms are carried out with the ANSYS program. Using the results of the elastic analysis, the progressive deformation and creep-fatigue damages are calculated step by step using the RCC-MR in detail. This paper will be a very useful guide for an actual application of the high temperature structural design of the nuclear power plant accounting for the time-dependent creep and stress-rupture effects.

Key Words : liquid metal reactor, high temperature design, creep-fatigue damage, progressive deformation, elastic follow-up, RCC-MR code

1. Introduction

In generating electricity by using atomic energy, there are many types of nuclear power plants such as the PWR(Pressurized Water Reactor), HTGR(High Temperature Gas Cooled Reactor), LMFBR(Liquid Metal Fast Breed Reactor), and so on. Generally, the operating temperature of a conventional PWR is under 350℃ and the operating pressure is quite high, over 150bar. Even though the operating pressure is high in these types, the creep or ratcheting behavior is not severe in the reactor internal structures for this temperature range. However, for most LMFBRs, the operating temperature exceeds 500℃ and the design pressure is low, under 5bar. Even though

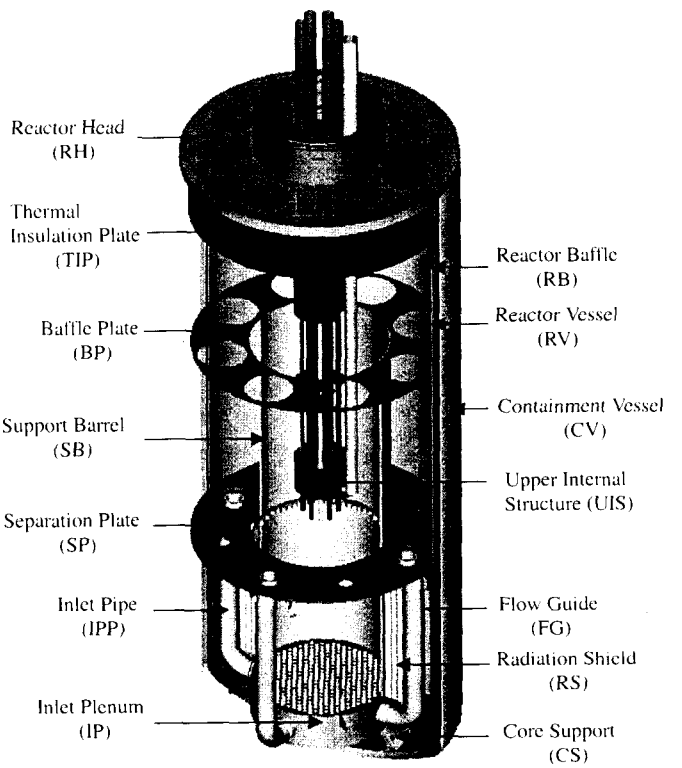

Fig. 1. Conceptually Designed KALIMER Reactor Internal Structures

the LMFBR has a great advantage such that any structural deterioration is progressive, not sudden due to lower operating pressure, the time dependent creep and ratchet behavior can severely occur in the reactor internal structures due to high temperature operation. In high temperature structural design, the parameters such as hold temperature, hold duration, and number of stress cycles are very important to evaluate the progressive deformation damage and creep-fatigue damage. Unlike the PWR design, these time dependent factors should be carefully considered in the stages of the design by analysis[1,2].

The RCC-MR[3] code used in this paper was developed in France, only for the purpose of LMFBR design subjected to high temperatures. The French design and construction rules for the mechanical components of an LMFBR nuclear island (RCC-MR) published in code form by AFCEN is primarily applied to safety class components. The design rules given in the RCC-MR are drafted jointly by the AFCEN and the Tripartite Committee. This committee was created on March 16th, 1978 by the Novatome to set up the rules applicable to the design of components operating at high temperature[3].

Like the ASME[4,5] and BDS[6] code, the RCC-MR provides two methods such as the elastic analysis method and the inelastic analysis method in evaluating creep-fatigue damage. The former method is very easy in calculating the stress and strain values but may give conservative results for the progressive deformation and creep-fatigue damage.

In this paper, the progressive deformation and creep-fatigue damage of the reactor internal structures of KALIMER(Korea Advanced LIquid MEtal Reactor), which is in the conceptual design stage, are evaluated using the elastic analysis method in the RCC-MR code for the thermal loads of normal operation, the seismic load OBE and the dead weight. The application procedure of the elastic analysis method in the RCC-MR code is clearly established in this paper. Actually, the basic concepts evaluating high temperature structures by the elastic analysis method in RCC-MR and the ASME Code Case N201-4 are similar, but the calculation procedure of RCC-MR is simpler than that of ASME Code Case N201-4. For the creep-fatigue damage evaluation, RCC-MR is based on the stress values while ASME is based on the strain values obtained from the elastic analysis[8]. The calculated creep-fatigue damage by RCC-MR for the KALIMER reactor internal structures is compared with that of ASME Code Case N201-4[7,8].

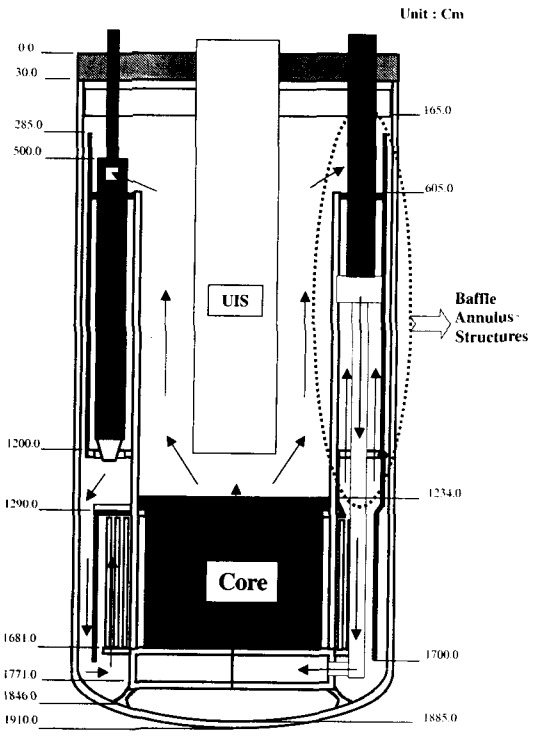

Fig. 2. Elevation of KALIMER Reactor Internal Structures

2. Elastic Analysis for Stress Calculations

2.1. Thermal Stress Analysis

The KALIMER reactor internal structures are composed of the Core Support Structure, Inlet Plenum, Support Barrel, Reactor Baffle, Baffle Plate, Separation Plate, Flow Guide, EMP Nozzle, Inlet Pipe, and Radiation Shield Structures. Fig. 1 shows the assembled reactor internal structures including the containment vessel, reactor vessel, reactor internal structures, and components. The annulus type internal structure called the baffle annulus shown in the schematic drawing of Fig. 2, which is composed of Reactor Baffle, support barrel, baffle plate, and separation plate, is provided to mitigate the large thermal gradients generated between hot and cold sodium boundaries. The temperature of stagnant sodium in the baffle annulus is steadily stratified at all operating conditions and will greatly reduce the thermal stress of the boundary regions of hot and cold sodium. Table 1 presents the conceptually designed dimension values of the reactor internals of KALIMER.

The heat transfer analysis for normal operation is performed to obtain the thermal gradients of the metal for the bulk temperature of sodium coolant flowing around the baffle annulus structures. Radial and axial thermal gradients of the reactor internal structures in the baffle annulus region are calculated using the finite element method with an axisymmetric analysis model bounded by elevations of 165cm and 1500cm in the axial direction in Fig. 2. The elevation of 165cm is the location of the bottom end of the thermal

Table 1. Dimensions of Conceptually Designed KALIMER Reactor Structures

Items	Outer Dia. (Cm)	Thickness (Cm)	Material	Remark (Cm)
1. Containment Vessel	737.0	2.5	2(1/4)Cr-1Mo	Partial-spherical bottom head
2. Reactor Vessel	702.0	5.0	316SS	Gap between RV and CV = 15.0
3. Reactor Baffle	687.0	2.5	316SS	Gap between RB and RV = 2.5
4. Support Barrel	374.0	5.0	316SS	Gap between SB and IHX = 16.925
5. Inlet Plenum	374.0	15.0	304SS	Upper Grid Plate T=10.0
				Lower Grid Plate T=15.0
6. Baffle Plate	687.0	2.5	316SS	Lower Baffle Plate T=2.5
				Upper Baffle Plate T=2.5
7. Separation Plate	687.0	10.0	316SS	Circular Disk Type
8. Core Support	374.0(t)	15.0	316SS	Skirt Type, Height=60
		454.0(b)		
9. Core	344.0	-	-	Gap between Core and SB = 10.0
10. Reactor Head	737.0	30.0	304SS	Circular Disk Type
11. Flow Guide	660.0	2.5	304SS	
12. Inlet Pipe	45.08	2.54	316SS	4 EA
13. Core Shield	248.0	15x3	316SS	3-Cylinder Type, Gap=3
				Height=370
14. Former Ring	358.0	10.0	316SS	
15. EMP Nozzle	125.0	2.5	316SS	Height=80

* O.D. of IHX (4EA) = 120 cm
* O.D. of EM-Pump (4EA) = 120 cm
* T : Thickness
* t, b : top, bottom

insulation plate. Fig. 3 shows the schematic drawing of the heat transfer mechanism assumed in the analysis. As shown in the figure, the baffle annulus region of the internal structures presents a very complex heat transfer mechanism including conduction, convection, and heat radiation. The convection heat transfer is applied to the support barrel inner surface, the baffle plate upper surface, the inner surface of the reactor baffle from the elevation of the baffle plate upper surface to the hot sodium free surface at an elevation of 315cm. The surfaces contacting the cold pool region, which are the inner surface of the reactor vessel and outer surface of the support barrel from the elevations of 1200cm to 1500cm and the flow guide surfaces have the convection heat transfer with the bulk temperature of the cold pool. Above the sodium free surfaces of the hot and cold pool, heat transfer across this region is by radiation only, as convection is assumed to be negligible. In this region, the radiation mechanism is assumed as an open system with a cover gas temperature of 430°C for steady state full power operation and 100°C for the refueling condition. The conduction heat transfer occurs across the stagnant sodium inside of the baffle annulus structure to the reactor

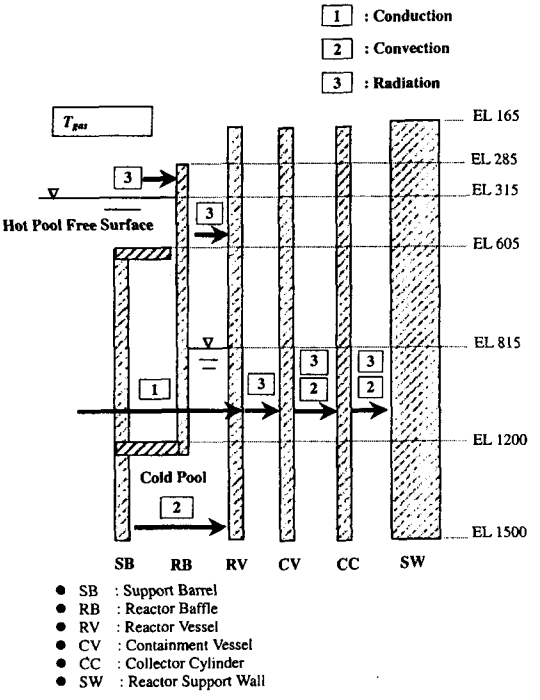

Fig. 3. Heat Transfer Mechanism Used in the Analysis

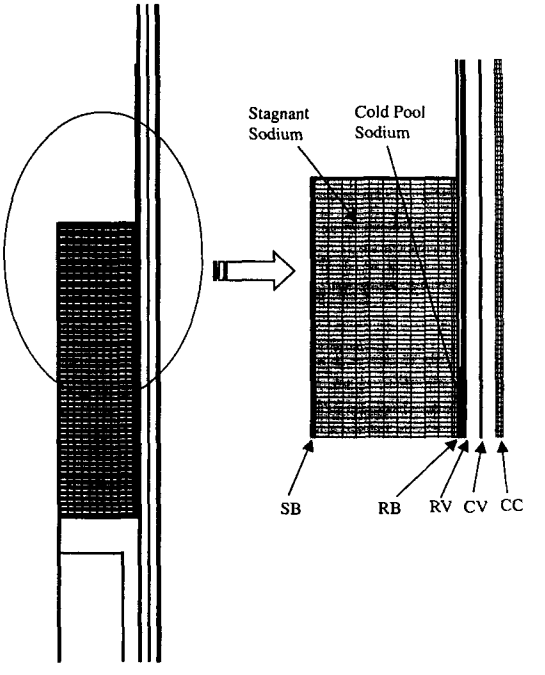

Fig. 4. Axisymmetric Finite Element Model of the Baffle Annulus in Reactor Internal Stuctures

baffle. The conduction heat transfer also occurs between the reactor baffle and reactor vessel through the cold pool sodium inside of the annulus. The reactor vessel is thermally coupled to the containment vessel only by radiation heat transfer. Both convection and radiation are included in the analysis between the containment vessel and the PSDRS collector cylinder. The radiation between the reactor vessel and the containment vessel, and between the containment vessel and the PSDRS collector cylinder, is treated as a closed system.

Fig. 4 shows an axisymmetric analysis model, which includes the reactor vessel, the containment vessel, and the PSDRS collector cylinder considering the heat transfer in the radial direction. The ANSYS 5.6 computer code[9] is used with STIFF 55 two-dimensional isoparametric thermal conduction and convection elements representing the structures and sodium, and with LINK32 element providing the 3-dimensional radiation links across the structural gaps where sodium is not filled. As shown in the analysis model, the element size is enough to produce accurate results for radiation, which is very sensitive to element size.

The calculated temperature distributions of the whole baffle annulus structure including the metal and sodium for steady state operation are shown in Fig. 5(a). From the results, the stagnant sodium inside the baffle annulus structure has a good function to make a stratified temperature distribution, which results in a significant reduction of the thermal gradient and heat loss in the boundary structures separating the hot and cold pool.

Fig. 5(b) shows the thermal stress distributions and the selected sections for calculation of stress

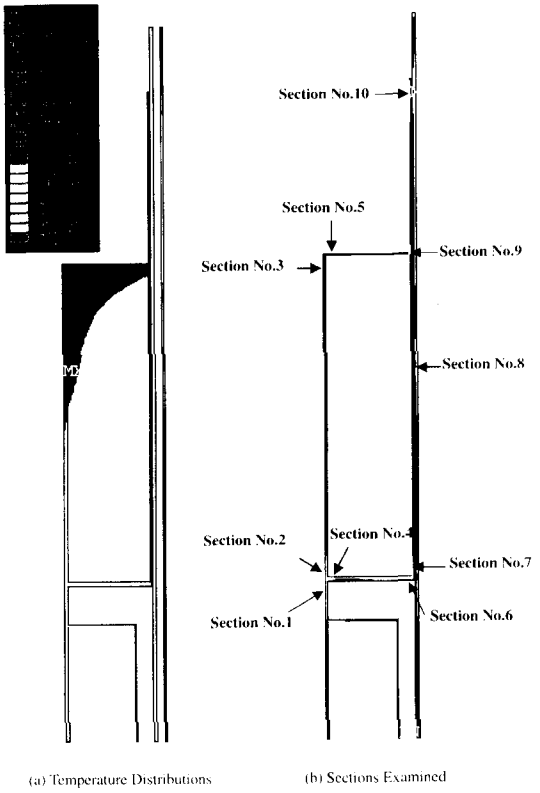

Fig. 5. Elastic Analysis Results for Steady State Normal Operation

intensities. As expected from the results of the thermal analysis, the thermal stresses significantly occurred at the junction part between the support barrel and the separation plate, and the junction part between the reactor baffle and the separation plate. Also, large thermal stress occurred at the reactor baffle in the region of the cold pool free surface region, the baffle plate elevation, and the hot pool free surface. Even high thermal stress occurred at the lower part of the support barrel below the separation plate elevation and the junction part between the reactor baffle and the separation plate, and these parts did not experience high temperatures during the steady state operation. Therefore, it is expected that there is no severe creep and ratcheting damage invoking the inelastic strain accumulation for the total service lifetime. Table 2 shows the calculated wall-averaged temperature and the maximum secondary stress intensities(membrane, bending, membrane plus bending) and peak stress components for each section.

In the structural evaluations, the stress caused by the circumferential thermal gradients is assumed to

Table 2. Maximum Stress Intensity for the Thermal load of Normal Operation, *MPa*

Section No. (Node-Node)	T_{max} (°C)	P_m	P_b	P_m+P_b	P_p	P_{total}
No. 1 (458-976)	404	34.7	69.9	103.6	1.0	103.6
No. 2 (481-993)	430	80.0	36.3	110.2	3.6	108.9
No. 3 (797-1239)	530	2.1	5.7	6.5	1.2	6.6
No. 4 (1332-1344)	400	10.7	27.9	35.0	1.4	34.0
No. 5 (2111-2474)	530	3.0	3.3	5.0	0.0	5.0
No. 6 (2502-2506)	386	28.3	22.7	50.6	12.3	57.4
No. 7 (2510-2748)	380	51.2	87.8	105.0	1.7	105.7
No. 8 (2509-2747)	430	6.5	11.1	17.5	0.4	17.4
No. 9 (2729-3077)	530	25.1	41.1	49.3	1.1	49.7
No.10 (3136-3086)	530	101.9	101.4	156.6	4.8	157.9

Table 3. Maximum Stress Intensity for an OBE Load, *MPa*

Section No.	*Pm*	*Pb*	*Pm+Pb*	*Pp*	*Ptotal*
No. 1	16.9	18.4	25.6	0.8	25.4
No. 2	14.0	47.1	47.9	2.0	49.8
No. 3	1.7	4.8	5.0	0.31	5.3
No. 4	1.55	34.9	35.5	0.5	36.0
No. 5	1.7	32.9	33.8	0.1	33.8
No. 6	0.8	11.6	11.8	6.2	15.0
No. 7	14.4	51.8	53.9	0.8	54.6
No. 8	0.6	0.0	0.6	0.0	0.6
No. 9	0.3	0.0	0.3	0.0	0.3
No.10	0.03	0.0	0.03	0.0	0.03

Table 4. Maximum Stress Intensity for Dead Weight, *MPa*

Section No.	*Pm*	*Pb*	*Pm+Pb*	*Pp*	*Ptotal*
No. 1	10.9	11.9	16.5	0.5	16.4
No. 2	9.0	30.4	30.9	1.3	32.1
No. 3	1.1	3.1	3.2	0.2	3.4
No. 4	1.0	22.5	22.9	0.3	23.2
No. 5	1.1	21.2	21.8	0.08	21.8
No. 6	0.5	7.5	7.6	4.0	9.7
No. 7	9.3	33.4	34.8	0.5	35.2
No. 8	0.4	0.0	0.4	0.0	0.4
No. 9	0.2	0.0	0.2	0.0	0.2
No.10	0.02	0.0	0.02	0.0	0.02

be negligible.

2.2. Seismic Stress for an Operating Basis Earthquake (OBE)

To obtain the seismic stress for OBE loads, a quasi-static analysis is performed for the maximum peak acceleration responses in the horizontal direction, 0.075g, and vertical direction, 1.55g, obtained from a detailed seismic time history analysis[10]. Table 3 is the calculated maximum primary stress intensities(membrane, bending, membrane plus bending) and peak stress for an OBE load. From the results, it is shown that large seismic stress occurred at the junction part between the support barrel and the separation plate, and the junction part between the reactor baffle and the separation plate. The bending stress is dominant due to a vertical seismic load.

2.3. Stress for Dead Weight

The stress for dead weight is calculated to check the structural integrity of the design load. Table 4 shows the calculated maximum primary stress intensities(membrane, bending, membrane plus bending) and peak stress for each section of interest.

3. Evaluations of Creep-Fatigue Damage Using RCC-MR

In the design of KALIMER reactor internal structures, normally operating at high temperatures over 500℃, for a design lifetime of 30 years, it is essential to consider the creep and stress-rupture effects in the stage of conceptual structure design.

The rules of RB-3200 in RCC-MR Subsection-B for Class 1 Components are used in the creep-fatigue evaluations of the reactor internal structures. When creep behavior is significant at the interesting points of the structures, the progressive deformation and the creep-fatigue damages can be evaluated according to RB-3262, the rules for the prevention of S type damage with the calculation results of the elastic analysis.

In this paper, the time-dependent damages are calculated for only the sections having wall-averaged temperatures over 430℃ , which are in the range of the creep temperature.

3.1. Limitation of Progressive Deformation Damage

In high temperature structural design, it is very important to prevent progressive damage in the points of functional requirements and structural integrity. When creep is negligible and purely elastic and plastic behavior are assumed, progressive deformation or ratchet is easily defined as an increase of deformation appearing at each cycle load. However, when creep is considered, i.e., the time-dependent phenomena, the progressive deformation designates the increase in deformation due to loads caused by imposed cyclic deformation. In other words, it is defined as the increase in deformation caused by creep when there is cyclic deformation, such as thermal deformation.

To accommodate this damage, ASME Subsection NH and Code Case N-201-4 provide the rules of the total accumulated inelastic strain limits for the design life time, 1.0% for base metal and 0.5% for weld metal. However, differing from the ASME design code, the RCC-MR code provides the rule of creep usage fraction associated with the effective primary membrane stress intensity and the effective primary stress intensity corrected by the creep effect.

In calculating the effective primary stress intensity, it is necessary to obtain the two parameters such as the secondary ratio and efficiency index. The former is the relative variation in secondary stress in relation to the primary stress being analyzed. The latter can be obtained using the calculated secondary ratio from an efficiency diagram as given in RCC-MR(figure RB 3262.1.1.2).

The secondary ratio in relation to the primary membrane stress intensity(Pm) is determined as follows;

$$SR_1 = \overline{\Delta Q} / (Max\, P_m), \tag{1}$$

where $\overline{\Delta Q}$ is the secondary stress range. The secondary ratio in relation to the sum of the primary stress intensities is determined as follows;

$$SR_3 = \overline{\Delta Q} / Max(P_L + \phi P_b). \tag{2}$$

In equation (2), P_L is the local primary membrane stress defined as $P_L = P_m + L_m$, where L_m is the mechanical stress occurring in a small zone adjoining the discontinuity due to the mechanical load such as the elastic follow-up. All symbols used in this paper are same in RCC-MR to make easy the understanding of the code procedures.

Table 5 shows the determined maximum primary stress intensities for normal operation. In this table, the thermal-induced membrane stress is

Table 5. Maximum Stress Intensity for Checking Progressive Deformation Damage, *MPa*

Section No. (Node-Node)	T_{max} (℃)	Max P_m	Max P_b	Max$(P_L+\phi P_b)$	Max ΔQ
Upper SB/SP (No. 2)	430	89.0	30.4	111.5	36.3
SB/BP (No. 3)	530	3.3	3.1	5.6	5.7
BP/SB (No. 5)	530	4.1	21.2	19.8	3.3
RB-Cold Free (No. 8)	430	6.9	0.0	6.9	11.1
RB at BP Elev. (No. 9)	530	25.3	0.0	25.3	41.1
RB- Hot Free (No.10)	530	101.9	0.0	101.9	101.4

Note that ϕ = 0.74 (circular cross-section beam) is used.

classified as primary stress with the assumption of the elastic follow-up exit[3,4,5].

Once the efficiency indices, V_1 and V_3, are known from the efficiency diagram using SR_1 and SR_3, the effective stress intensities can be obtained as follows;

$$P_1 = Max\, P_m / V_1, \quad (3)$$

$$P_3 = Max(P_L + \phi P_b)/V_3. \quad (4)$$

In equation (4), coefficient ϕ depends on the geometry of the cross-section concerned. It is equal to 0.8 for plate elements and thin-wall shells with rectangular cross section, 0.88 for circular cross-section tube, 0.74 for circular cross-section beam, and 0.66 for square cross-section beam and bending in plane of a diagonal.

Finally, the limits of the progressive deformation damage can be checked using the creep usage fractions as follows;

$$U_1 = \sum_{j=1}^{N} U_A[t_j / T_j(P_1/1.2)] \le 1.0, \quad (5)$$

$$U_3 = \sum_{j=1}^{N} U_A[t_j / T_j(P_3/1.2)] \le 1.0. \quad (6)$$

In equations (5) and (6), t_j is the service time for j stress cycle and the maximum allowable time T_j is determined based on the maximum allowable stress, S_t, curves given in A.3.5.2 of RCC-MR.

Table 6 shows the results of the calculated total creep usage fraction for the high temperature structural parts in the KALIMER reactor internal structures and the satisfaction of the limit rule of the progressive deformation damage for normal operation. In this check, the earthquake load is excluded from the load combination due to the rapid dynamic phenomena and is thus a negligible effect for creep damage. From the results, all sections examined satisfy the limit criteria of progressive deformation. However, section no.10, Reactor Baffle at the hot sodium free surface, shows a very high creep usage fraction of 0.657 with little design margin due to a large primary stress intensity at high temperatures.

Table 6. Evaluation Results of the Progressive Deformation Rule in RCC-MR

Section No.	Secondary Ratio		Efficiency Index		Effective Stress Int.		Creep Usage Fraction	
	SR_1	SR_3	V_1	V_3	P_1	P_3	$U_A(P_1/1.2) < 1$	$U_A(P_3/1.2) < 1$
No. 2	0.408	0.326	1.00	1.00	89.0	111.5	0.044	0.066
No. 3	1.781	1.018	0.70	0.85	4.6	6.6	0.000	0.000
No. 5	1.065	0.167	0.85	1.00	4.8	19.8	0.000	0.026
No. 8	1.609	1.609	0.75	0.75	9.2	9.2	0.000	0.000
No. 9	1.625	1.625	0.74	0.74	34.2	34.2	0.044	0.044
No.10	0.995	0.995	0.86	0.86	118.5	118.5	0.657	0.657

3.2. Limitation of Creep-Fatigue Damage

When the metal undergoes high temperature conditions, the creep damage and fatigue damage cannot be treated separately in fracture failure. In high temperature conditions, the severe interaction between the creep and fatigue occurs and it causes a significant reduction of the numbers and hold times at high temperature operation. The following equation presents the limit rule of the accumulated creep and fatigue damage for the total design lifetime.

$$\sum_{j=1}^{p}\left(\frac{n}{N_d}\right)_j + \sum_{k=1}^{q}\left(\frac{t}{T_d}\right)_k \le D \qquad (7)$$

where

D = total creep-fatigue damage

P = number of different cycle types

$(n)_j$ = number of applied repetitions of cycle type, j

$(N_d)_j$ = number of design allowable cycles for cycle type, j

q = number of time intervals for the creep damage calculation

$(T_d)_k$ = allowable time duration determined from the stress-to-rupture curves

The check on the resistance to the damage resulting from the accumulation of the effects of creep and fatigue consists in demonstrating that at all points of the structure and for all the stress cycles for which compliance with Level A criteria is required. The representative points defining the coordinates of creep and fatigue values shall be located within an allowable area defined on creep-fatigue interaction diagrams as shown in Fig. 6.

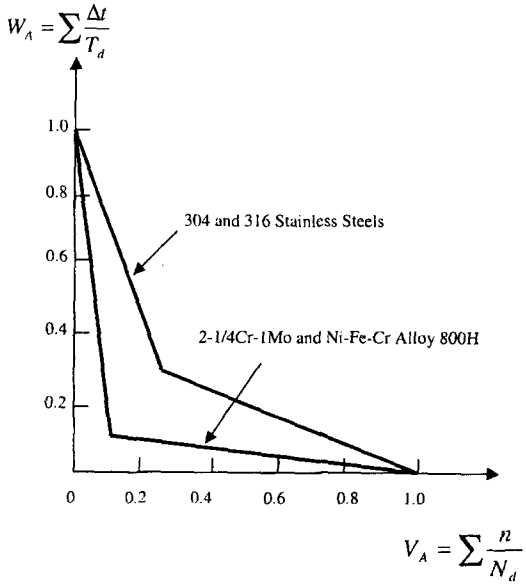

Fig. 6. Creep-Fatigue Interaction Curves

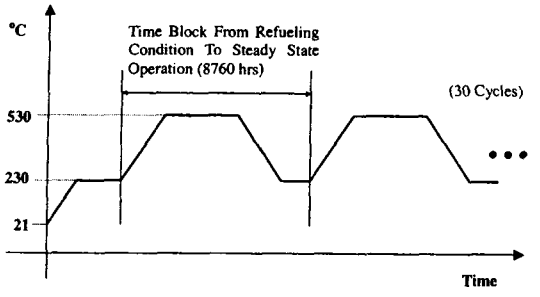

Fig. 7. Assumed Normal Operation Cycles Used in the Evaluation

3.2.1. Load Combinations and Stress Cycles

Fig. 7 shows the assumed time history of the bulk temperature of reactor coolant for normal operating condition. The hold time duration for one cycle is conservatively assumed as 8760 hours from heat-up to cool-down operation corresponding to the assumed refueling period of one year. Therefore, the total number of cycles for this operation becomes 30 when considering a 30 year design lifetime of the reactor system.

Five of the OBE(Operating Basis Earthquake) are assumed to occur during the worst Level A service conditions and each earthquake is assumed to contain 10-peak acceleration cycles. Therefore, in calculating the fatigue damage, the stress caused by an OBE load will be combined with those of the thermal loads in determination of the maximum stress ranges for 5 stress cycles among 30 cycles of thermal load. Consequently, the load combinations and related stress cycles for the fatigue damage considered in the paper are as follows;

Thermal Load + OBE + Dead Weight = 5 Cycles,
Thermal Load + Dead Weight = 25 Cycles,
OBE = 50 Cycles .

For the creep damage calculations, the OBE is not considered because rapid dynamic phenomena occurring in a short time have no serious effects on progressive deformation depending on the time duration.

3.2.2. Calculation of Fatigue Damage : $V_A\,\overline{(\Delta\varepsilon)}$

In high temperature structural design, the failure mechanism follows the low cycle fatigue model due to large inelastic strain variation including creep strain for both thermal and mechanical loads. Thus, the total strain range must be calculated for calculation of fatigue damage.

The total strain ranges including the amplification of strain due to plasticity, $\overline{(\Delta\varepsilon)}_{el+pl}$ and creep, $\overline{\Delta\varepsilon}_{cr}$ can be obtained from the results of stresses obtained by an elastic analysis as follows;

$$\overline{\Delta\varepsilon} = \overline{(\Delta\varepsilon)}_{el+pl} + \overline{\Delta\varepsilon}_{cr} . \qquad (8)$$

In equation (8), the elastic plus plastic strain range, $\overline{\Delta\varepsilon}_{el+pl}$ can be obtained using the sum of the four strain components considering the amplification due to plasticity, as follows;

$$\overline{(\Delta\varepsilon)}_{el+pl} = \overline{\Delta\varepsilon}_1 + \overline{\Delta\varepsilon}_2 + \overline{\Delta\varepsilon}_3 + \overline{\Delta\varepsilon}_4 . \qquad (9)$$

These four components are determined using the Cyclic Curve(A.3.5.9 of RCC-MR) corresponding to the highest temperature at the point examined during the cycle concerned. Note that all units of stress and strain in applying the RCC-MR are *MPa* and percent(%) respectively.

The in equation (9) represents the strain range calculated on the basis of the total stress intensity range, $\Delta\sigma_{tot} = \Delta(\overline{P+Q+F})$ obtained from the elastic analysis as shown in Fig. 8. This strain component can be obtained by a simple equation as follows;

$$\overline{\Delta\varepsilon}_1 = \frac{2}{3}(1+\nu)(\overline{\Delta\sigma}_{tot} / E), \qquad (10)$$

Table 7. Calculated Total Stress Range for Thermal Load, *MPa*

Section No.	$\sigma_1(t)$	$\sigma_2(t)$	$\sigma_3(t)$	$\sigma_1(t')$	$\sigma_2(t')$	$\sigma_3(t')$
No. 2	5.620	-0.154	-4.418	21.220	-0.707	-82.600
No. 3	0.004	-1.358	-1.629	0.018	-5.589	-6.311
No. 5	0.314	-0.014	-0.827	1.266	-0.045	-3.522
No. 8	8.173	1.212	1.006	19.300	7.323	2.423
No. 9	-0.302	-7.485	-8.761	-1.797	-40.610	-49.420
No.10	80.320	1.108	-38.300	99.74	2.371	-41.800

Table 8. Calculated Total Stress Range for Thermal Load, *MPa*

Section No.	$S_1(t)$	$S_2(t)$	$S_3(t)$	$S_1(t')$	$S_2(t')$	$S_3(t')$	$\overline{\sigma(t,t')}$
No. 2	5.271	-0.503	-4.767	41.916	19.989	-61.904	96.497
No. 3	0.998	-0.364	-0.635	3.979	-1.628	-2.350	4.488
No. 5	0.490	0.162	-0.651	2.033	0.722	-2.755	3.268
No. 8	4.709	-2.252	-2.458	9.618	-2.359	-7.259	8.411
No. 9	5.214	-1.969	-3.245	28.812	-10.001	-18.811	35.993
No.10	65.944	-13.268	-52.676	79.636	-17.733	-61.904	20.949

where υ is Poisson ratio and E is the elastic modulus. When applying the rules of RCC-MR, the stress intensity and the stress range can be determined using one of two methods among the maximum shear method and the octahedral shear method. In this paper, the latter method is used in calculating the total stress intensity range, $\overline{\Delta\sigma_{tot}}$ in equation (10).

According to the octahedral shear method, the stress deviator S(t) can be expressed as a function of the principal components as follows;

$$S_1(t) = \sigma_1(t) - [\sigma_1(t)+\sigma_2(t)+\sigma_3(t)]/3 \quad , \tag{11}$$

$$S_2(t) = \sigma_2(t) - [\sigma_1(t)+\sigma_2(t)+\sigma_3(t)]/3 \quad , \tag{12}$$

$$S_3(t) = \sigma_3(t) - [\sigma_1(t)+\sigma_2(t)+\sigma_3(t)]/3 \quad , \tag{13}$$

where $\sigma_1(t)$,$\sigma_2(t)$, and $\sigma_3(t)$ are the principal stresses. From equations (11) to (13), the stress intensity range can be calculated for each pair of time points (t) and (t') of the stress cycle as follows;

$$\overline{\Delta\sigma(t,t')} = \sqrt{3/2}\cdot\left\{[S_1(t)-S_1(t')]^2+[S_2(t)-S_2(t')]^2 + [S_3(t)-S_3(t')]^2\right\}^{1/2}. \tag{14}$$

Table 7 shows the principal stress for total stress obtained from two time points assuming to produce the maximum stress range. In this paper, time point (t) represents the refueling condition 230°C of all primary sodium pools in the reactor vessel and time point (t') represents the steady state normal operating condition in one stress cycle as shown Fig. 7. Table 8 is the calculated stress deviators and the total stress intensity range.

Table 9 shows $\overline{\Delta\varepsilon_1}$ calculated at the high temperature points examined. For creep damage evaluation, the stress due to an OBE load is not included, but for fatigue damage evaluation this is included. All values without parentheses in the table indicate no OBE load is included for creep damage evaluations and all values with parentheses in the table indicate that an OBE load is included for fatigue damage evaluations.

The $\overline{\Delta\varepsilon_2}$ in equation (9) represents the plastic strain increment associated with the primary stress intensity range at the point examined as shown in Fig. 8, equal to

Table 9. Calculated Strain Component for Creep-Fatigue Damage

Section No.	Tmax, ℃	υ	E, GPa	$\overline{\Delta\sigma_{tot}}$, MPa	$\overline{\Delta\varepsilon_1} = \frac{2}{E}(1+\upsilon)\overline{\Delta\sigma_{tot}}$, %
No. 2	430	0.3	158	96.497(*)	0.0529
				(146.297)(**)	(0.0803)
No. 3	530	0.3	150	4.488	0.0026
				(9.788)	(0.0057)
No. 5	530	0.3	150	3.268	0.0019
				(37.068)	(0.0214)
No. 8	430	0.3	158	8.411	0.0046
				(9.011)	(0.0049)
No. 9	530	0.3	150	35.993	0.0208
				(36.293)	(0.0210)
No.10	530	0.3	150	20.949	0.0121
				(20.979)	(0.0121)

(*) : without OBE loads for creep damage
(**) : with OBE loads for fatigue damage

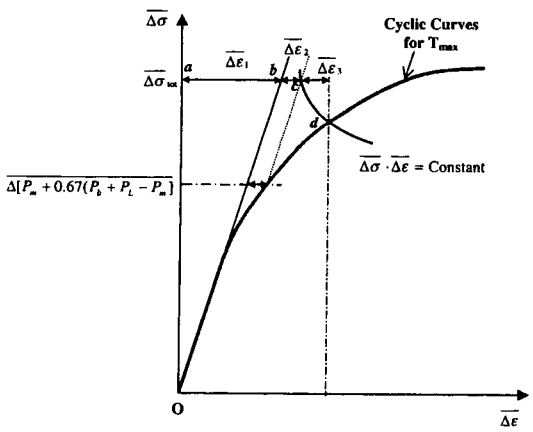

Fig. 8. Diagram of Determination of the Strain Range Components

$$\overline{\Delta\varepsilon_2} = \overline{\Delta\varepsilon_p}\left(\Delta[P_m + 0.67(P_b + P_L - P_m)]\right) \quad (15)$$

This plastic strain increment can be obtained from a formulation of the Cyclic Curves of A3.5.9 in RCC-MR as follows;

$$\overline{\Delta\varepsilon_2} = \left\{\frac{\Delta[P_m + 0.67(P_b + P_L - P_m)}{K}\right\}^{(1/m)} \quad (16)$$

where K and m are the coefficients depending on temperature. In this paper, the membrane stress associated with the thermal load is classified into the general primary membrane stress, P_m, but not the local primary membrane stress L_m with the assumption that this stress will be not relaxed after small scale deformation because of elastic follow-up. The primary stress intensity range due to the thermal load is calculated with the procedures of above equations (11) to (14) and the OBE stresses are combined algebraically with those of the thermal load for the fatigue damage evaluations. Table 10 and Table 11 are the calculated principal stress and the maximum primary stress intensity range at two time points. Table 12 shows the calculated strain component $\overline{\Delta\varepsilon_2}$ using equation (16).

The $\overline{\Delta\varepsilon_3}$ in equation (9) represents the plastic strain increment along path (c-d) of Fig. 8 applying Neuber's Rule. In the figure, point (d) is the intersection point of the Cyclic Curve and the hyperbola $\overline{\Delta\sigma} \cdot \overline{\Delta\varepsilon} = Const$ passing through point (c) with coordinates, { $\overline{\Delta\varepsilon_1} + \overline{\Delta\varepsilon_2}$; $\overline{\Delta\sigma_{tot}}$ }. This procedure may be somewhat complicated. Alternatively, as a simpler procedure, $\overline{\Delta\varepsilon_3}$ can be obtained from the following simple equation when

Table 10. Calculated Primary Membrane Stress Range for Thermal Load, MPa

Section No.	$\sigma_1(t)$	$\sigma_2(t)$	$\sigma_3(t)$	$\sigma_1(t')$	$\sigma_2(t')$	$\sigma_3(t')$
No. 2	0.705	-0.483	-4.579	6.948	-5.003	-69.220
No. 3	0.043	-0.057	-0.425	0.167	-0.219	-1.811
No. 5	0.005	-0.270	-0.562	0.021	-1.160	-2.766
No. 8	3.177	0.032	-0.051	6.138	0.162	-0.187
No. 9	0.066	-0.086	-4.118	0.402	-0.520	-23.520
No.10	1.640	-1.469	-72.520	2.734	-2.474	-95.080

Table 11. Calculated Primary Membrane Stress Range for Thermal Load, MPa

Section No.	S1(t)	S2(t)	S3(t)	S1(t')	S2(t')	S3(t')	$\overline{\Delta P_m(t,t')}$
No. 2	2.157	0.969	-3.127	29.373	17.422	-46.795	66.162
No. 3	0.189	0.089	-0.279	0.788	0.402	-1.190	1.389
No. 5	0.281	0.006	-0.286	1.323	0.142	-1.464	1.933
No. 8	2.124	-0.021	-1.104	4.100	-1.876	-2.225	3.592
No. 9	1.444	1.292	-2.740	8.281	7.359	-15.641	19.365
No.10	25.756	22.647	-48.404	34.341	29.133	-63.473	22.678

Table 12. Calculated Strain Component $\Delta\varepsilon_2$ for Creep-Fatigue Damage

Section No.	T_{max}, °C	$\overline{\Delta[P_m+0.67(P_b+P_L-P_m)]}$, *MPa*	K	m	$\overline{\Delta\varepsilon_2}=(\overline{\Delta\sigma}/K)^{(1/m)}$, %
No. 2	430	66.162 (111.719)	677	0.378	2.13E-3 (8.51E-3)
No. 3	530	1.389 (6.305)	739	0.326	4.35E-9 (4.50E-7)
No. 5	530	1.933 (25.676)	739	0.326	1.20E-8 (3.34E-5)
No. 8	430	3.592 (4.192)	677	0.378	9.57E-7 (1.44E-6)
No. 9	530	19.365 (19.665)	739	0.326	1.41E-5 (1.48E-5)
No.10	530	22.678 (22.708)	739	0.326	2.28E-5 (2.29E-5)

* K and m : coefficients depending on temperature (A.3.5.9 in RCC-MR)

is negligible $\overline{\Delta\varepsilon_1}$.

$$\overline{\Delta\varepsilon_3} = (K_\varepsilon - 1.0)\overline{\Delta\varepsilon_1} \quad , \tag{17}$$

where K_ε is the amplification coefficient obtained from A3.5.9 in RCC-MR corresponding to $\overline{\Delta\sigma_{tot}}$ and the maximum temperature. As shown in Table 12, the calculated $\overline{\Delta\varepsilon_2}$ is very small and negligible, therefore a simple equation (17) is used in calculating $\overline{\Delta\varepsilon_3}$. Table 13 shows the calculated

Table 13. Calculated Strain Component $\overline{\Delta\varepsilon_3}$ for Creep-Fatigue Damage

Section No.	T_{max}, °C	$\overline{\Delta\sigma_{tot}}$, *MPa*	Kε	$\overline{\Delta\varepsilon_3}=(K_\varepsilon-1.0)\,\overline{\Delta\varepsilon_1}$,%
No. 2	430	96.497 (146.297)	1.045 (1.084)	2.381E-3 (6.745E-3)
No. 3	530	4.488 (9.788)	1.001 (1.001)	2.600E-6 (5.700E-6)
No. 5	530	3.268 (37.068)	1.001 (1.003)	1.900E-6 (6.420E-5)
No. 8	430	8.411 (9.011)	1.001 (1.001)	4.600E-6 (4.900E-6)
No. 9	530	35.993 (36.293)	1.003 (1.003)	6.240E-5 (6.300E-5)
No.10	530	20.949 (20.979)	1.002 (1.002)	2.420E-5 (2.420E-5)

• K_ε : Amplification Coefficient (A3.5.9 in RCC-MR)

values of $\overline{\Delta\varepsilon_3}$.

The $\overline{\Delta\varepsilon_4}$ in equation (9) represents the plastic strain increment due to triaxiality. This can be obtained by the following equation;

$$\overline{\Delta\varepsilon_4} = (K_v - 1.0)\,\overline{\Delta\varepsilon_1}, \qquad (18)$$

where K_v is the amplification coefficient, as a function of $\overline{\Delta\sigma_{tot}}$ and the maximum temperature, obtained from A3.5.9 in RCC-MR. Table 14 shows the calculated values of $\overline{\Delta\varepsilon_4}$.

Finally, the amplification of the strain range, $\overline{\Delta\varepsilon_{cr}}$ in equation (8), which results from creep, can be obtained by using the creep rule of A3.6.3 in RCC-MR to calculate the creep strain increment due to a stress equal to

$$\sigma_k = \text{Mean}\,\overline{P} + K_s\,\overline{\Delta\sigma^*} \qquad (19)$$

held for time duration t at the maximum temperature Tmax. In the above equation, the last term $\overline{\Delta\sigma^*}$ is obtained from the Cyclic Curve of A3.5.9 in RCC-MR corresponding to $\overline{\Delta\varepsilon_{el+pl}}$ calculated in equation (9). K_s is the symmetrization coefficient obtained from the curve of A3.5.7 in RCC-MR as a function of the following ratio R.

$$R = \overline{\Delta\sigma^*} / 2[R_{0.2\%}(T_{max})]_{min}, \qquad (20)$$

where $(R_{0.2\%})_{min}$ is the minimum 0.2% offset yield strength obtained from A.3.3.1 in RCC-MR as a function of temperature and independent of time.

The presence of a mean stress in the loading cycle, if the temperature is sufficiently high, may cause the creep strain continuously with time. Thus, a component subjected to both mean and alternating stresses must be designed to prevent the occurrence of both fatigue and creep failure, designated either by creep rupture or by some maximum permissible creep strain[11]. In the rules of RCC-MR, the mean value, during the cycle, of the primary stress intensity in equation (14) is defined as follows;

Table 14. Calculated Strain Component for Creep-Fatigue Damage

Section No.	T_{max}, °C	$\overline{\Delta\sigma_{tot}}$, *MPa*	K_v	$\overline{\Delta\varepsilon_4}=(K_v-1.0)\overline{\Delta\varepsilon_1}$,%
No. 2	430	96.497 (146.297)	1.037 (1.064)	1.957E-3 (5.139E-3)
No. 3	530	4.488 (9.788)	1.001 (1.001)	2.600E-6 (5.700E-6)
No. 5	530	3.268 (37.068)	1.001 (1.002)	1.900E-6 (4.280E-5)
No. 8	430	8.411 (9.011)	1.001 (1.001)	4.600E-6 (4.900E-6)
No. 9	530	35.993 (36.293)	1.002 (1.002)	4.160E-5 (4.200E-5)
No.10	530	20.949 (20.979)	1.002 (1.002)	2.420E-5 (2.42E-5)

• K_v : Amplification Coefficient (A3.5.9 in RCC-MR)

$$\text{Mean}\,\overline{P} = (1/t_k)\int_0^{t_k}\overline{[P_m+0.67(P_b+P_L-P_m)]}\,dt\,, \quad (21)$$

where t_k is the duration of the cycle considered. The duration of the cycle, considered in this paper, is 8750 hours. Most of this time is for normal steady state operation with full power. Thus, the mean $\overline{P}$ is conservatively determined as the maximum primary stress values combining the thermal load of the steady state and the dead weight. The stresses related with the OBE and the refueling condition are neglected because the hold times of these conditions are very short compared with that of steady state normal operation.

To calculate the creep strain increment associated with the stress of equation (14), the creep rule of A3.6.3 in RCC-MR can be applied as follows;

$$\overline{\Delta\varepsilon}_{cr} = C_1 T^{C_2}(\sigma_k)^{n_1}\,, \quad (22)$$

where coefficients C_1, C_2, and n_1 are function of the temperature given in A3.6.3.1. The time T shall be the stress cycle time-temperature block instead of the entire service lifetime.

Table 15 shows the calculated creep strain increments and the total stress. As shown in the table, the maximum $\overline{\Delta\varepsilon_{el+pl}}$, 0.1%, occurred at section no.2(junction of Support Barrel and Separation Plate) and the maximum $\overline{\Delta\varepsilon_{cr}}$, 0.04%, occurred at section no.10(Reactor Baffle section at the hot pool free surface). The mean primary stress intensity is very large at these sections due to the assumed risk of elastic follow-up.

For the fatigue damage evaluations, the maximum allowable number of cycles N_d corresponding to the calculated total strain range of cycle j is determined with the fatigue curves given in A3.6.3 of RCC-MR. Thus, the fatigue usage fractions $V_A(\overline{\Delta\varepsilon})$ shall be calculated as follows;

$$V_A(\overline{\Delta\varepsilon}) = \sum_{j=1}^{p}\left(\frac{n}{N_d}\right)_j\,, \quad (23)$$

where p is number of cycle types and n is number of applied repetitions of cycle type, j.

The calculated fatigue usage fractions for each section are shown in Table 16 and compared

Table 15. Calculated Creep Strain Component and Total Stress

Section No.	Mean $\overline{P}$, *MPa*	$\Delta\varepsilon_{el+pl}$, %	$\overline{\Delta\sigma^*}$, *MPa*	$(R_{0.2\%})_{min}$, *MPa*	R	K_s	σ_k, *MPa*	$\overline{\Delta\varepsilon_{cr}}$,%
No. 2	109.37	0.0594 (0.1007)	90 (140)	119	0.38 (0.59)	1.0 (0.891)	199.4 (235.0)	3.453E-3 (6.561E-3)
No. 3	5.28	0.0026 (0.0057)	5 (10)	114	0.02 (0.04)	1.0 (1.0)	10.3 (15.3)	0.0 (0.0)
No. 5	18.30	0.0019 (0.0215)	4 (40)	114	0.02 (0.18)	1.0 (1.0)	22.3 (58.3)	3.053E-5 (1.625E-3)
No. 8	6.90	0.0046 (0.0049)	10 (10)	119	0.04 (0.04)	1.0 (1.0)	16.9 (16.9)	0.0 (0.0)
No. 9	25.30	0.0209 (0.0211)	40 (40)	114	0.18 (0.18)	1.0 (1.0)	65.3 (65.3)	2.598E-3 (2.598E-3)
No.10	101.92	0.0122 (0.0122)	25 (25)	114	0.11 (0.11)	1.0 (1.0)	126.9 (126.9)	4.069E-2 (4.069E-2)

Table 16. Calculated Fatigue Usage Fractions

Sections	Fatigue Usage Fraction $V_A(\overline{\Delta\varepsilon_t}) = \sum_k V(\overline{\Delta\varepsilon_t})_k$				
	$\overline{\Delta\varepsilon_{el+pl}}$, %	$\overline{\Delta\varepsilon_{cr}}$, %	$\overline{\Delta\varepsilon_t}$, %	Calculated by	
				RCC-MR	ASME[8]
No. 2	0.1007	6.561E-3	0.1073	0.0	0.0
No. 3	0.0057	0.0	0.0057	0.0	0.0
No. 5	0.0215	1.625E-3	0.0231	0.0	0.0
No. 8	0.0049	0.0	0.0049	0.0	0.0
No. 9	0.0211	2.598E-3	0.0237	0.0	0.0
No.10	0.0122	4.069E-2	0.0529	0.0	0.002

with those of the ASME Code Case N-201-4[8]. The maximum allowable number of cycles corresponding to the calculated total strain range is over 1.0×10^6, which is very large compared with the number of the stress cycles mentioned in above section 4.3.1. Therefore, as shown in Table 16, the fatigue usage fraction can be negligible in KALIMER reactor internals for the normal operating conditions considered in this paper.

3.2.3. Calculation of Creep Damage : $W_A(\sigma_k/0.9)$

Finally, for the creep damage evaluations, the maximum allowable time, T_d, corresponding to the stress $(\sigma_k/0.9)$ is determined on the basis of the minimum value of the creep rupture stress, Sr,

Table 17. Calculated Creep Rupture Usage Fraction

Sections No.	Creep Rupture Usage Fraction $W_A(\sigma) = \sum_k W(\sigma_k/0.9)$					
	$(\sigma_k/0.9)$, MPa	Cycles	Hold Time per Cycle t_k, hours	Allowable $(T_d)_k$, hours	Calculated by RCC-MR	Calculated by ASME[8]
No. 2	221.56	30	8760	6×10^6	0.044	0.026
No. 3	11.44	30	8760	1×10^8	0.003	0.003
No. 5	24.78	30	8760	3×10^7	0.009	0.003
No. 8	18.78	30	8760	Over 1×10^8	0.0	0.0
No. 9	72.56	30	8760	3×10^6	0.088	0.088
No.10	141.00	30	8760	3.5×10^5	0.751	0.876

curves given in A.3.5.3 of RCC-MR. Thus, the creep rupture usage fractions $W_A(\sigma_k/0.9)$ shall be calculated as follows;

$$W_A(\sigma_k/0.9) = \sum_{k=1}^{q}\left(\frac{t}{T_d}\right)_k . \qquad (24)$$

The calculated creep rupture usage fractions for each section are shown in Table 17 and compared with those of the ASME Code Case N-201-4. As shown in this table, the results of the calculated creep damages using RCC-MR are very similar with those of the ASME. The maximum creep damage occurs at the Reactor Baffle section at the hot pool free surface.

3.2.4. Check of Creep-Fatigue Interaction Curve

Fig. 9 shows the representative points defining the coordinates of creep and fatigue values calculated in this paper on a creep-fatigue interaction diagram. All values are located within an allowable area but the creep rupture usage fraction values are too high and have little design margin. When the additional design transient loading conditions are considered in calculating the fatigue damage, it cannot assure that the

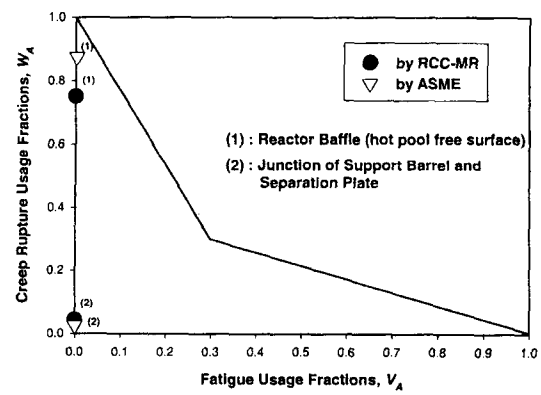

Fig. 9. Checking Results of the Creep-Fatigue Interaction Curve

KALIMER reactor internal structures subjected to high temperature conditions satisfy the design rules of RCC-MR or ASME.

4. Conclusions

In this paper, the accumulated progressive deformation and the creep-fatigue damage for normal operation during the total design lifetime are investigated using the RCC-MR code for the reactor internal structures of KALIMER subjected to high temperatures over 430℃. The results obtained by using RCC-MR are very similar with

those of the ASME design code. That means the elastic analysis methods using in the high temperature structural design of the nuclear power plant are basically on the similar concept and conservatism in both design codes.

All sections considered in this paper satisfy the creep-fatigue interaction curve given in the design rules of RCC-MR for normal operation. However, the design margin of the reactor baffle section on the elevation level of the hot pool free surface is so small due to its large creep damage value, 0.75. The main reason for this small margin is that the membrane stresses induced by the thermal load are classified as the primary stresses in this paper. Thus the mean primary stress intensity contributes significantly in calculating the creep rupture usage fraction. This is on the conservative assumption that the risk of the elastic follow-up may exist in this section due to the high metal temperature.

In checking the structural integrity of the high temperature design of the reactor internals of KALIMER, care should be taken for the existence of elastic follow-up and more detailed transient events related with the fatigue damage in normal operation.

Acknowledgment

This work has been carried out under the Nuclear R & D Program by MOST.

References

1. Creep-Fatigue Damage Rules for Advanced Fast Reactor Design, IAEA-TECDOC-933, IAEA, (1996).
2. L.K. Severud, "Creep-Fatigue Assessment Methods Using Elastic Analysis Results and Adjustments," Transactions of the ASME, Vol.113, pp.34-40, (1991).
3. RCC-MR, Design and Construction Rules for Mechanical Components of FBR Nuclear Islands, AFCEN, (1985).
4. ASME Boiler and Pressure Vessel Code Section III, Subsection NH, ASME, (1995).
5. Cases of ASME Boiler and Pressure Vessel Code, N-201-4, ASME, (1994).
6. Elevated Temperature Structural Design Guide for Class 1 Components of Prototype Fast Breeder Reactor, PNC N241-84-08, PNC, (1984).
7. G.H. Koo, H.Y. Lee, Y.S. Joo, et.al, "Thermal Stress Analysis and Service Limit Check for KALIMER Reactor Internal Structures," Proceedings of the Korean Nuclear Society Spring Meeting, (1999).
8. G.H. Koo and B. Yoo, "Elevated Temperature Design of KALIMER Reactor Internals Accounting for Creep and Stress-Rupture Effects," Journal of the Korean Nuclear Society, Vol.32, No.6, pp.566-594, (2000).
9. ANSYS User's Manual for Revision 5.6, Volume I and II.
10. G.H. Koo, Y.H. Lee, and B. Yoo, "Seismic Design and Analysis of Seismically Isolated KALIER Reactor Structures," Journal of the Earthquake Engineering Society of Korea, Vol.3. No.1, pp.75-92, (1999)
11. N.E. Frost, K.J. Marsh, and L.P. Pook, Metal Fatigue, Clarendon press, Oxford, (1974).